Particle Swarm Optimization-Based Metaheuristic Design Generation of Non-Trivial Flat-Foldable Origami Tessellations With Degree-4 Vertices

Yao Chen[1]
Associate Professor
Key Laboratory of Concrete and Prestressed Concrete Structures of Ministry of Education, and National Prestress Engineering Research Center,
Southeast University,
Nanjing 211189, China
e-mail: chenyao@seu.edu.cn

Jiayi Yan
School of Civil Engineering,
Southeast University,
Nanjing 211189, China
e-mail: jyyan_guuru@126.com

Jian Feng
Professor
National Prestress Engineering Research Center, and
Key Laboratory of Concrete and Prestressed Concrete Structures of Ministry of Education,
Southeast University,
Nanjing 211189, China
e-mail: fengjian@seu.edu.cn

Pooya Sareh
Creative Design Engineering Lab (Cdel),
School of Engineering,
University of Liverpool,
Liverpool, The Quadrangle,
Brownlow Hill, L69 3GH, UK
e-mail: pooya.sareh@liverpool.ac.uk

Flat-foldable origami tessellations are periodic geometric designs that can be transformed from an initial configuration into a flat-folded state. There is growing interest in such tessellations, as they have inspired many innovations in various fields of science and engineering, including deployable structures, biomedical devices, robotics, and mechanical metamaterials. Although a range of origami design methods have been developed to generate such fold patterns, some non-trivial periodic variations involve geometric design challenges, the analytical solutions to which are too difficult. To enhance the design methods of such cases, this study first adopts a geometric-graph-theoretic representation of origami tessellations, where the flat-foldability constraints for the boundary vertices are considered. Subsequently, an optimization framework is proposed for developing flat-foldable origami patterns with four-fold (i.e., degree-4) vertices, where the boundaries of the unit fragment are given in advance. A metaheuristic using particle swarm optimization (PSO) is adopted for finding optimal solutions. Several origami patterns are studied to verify the feasibility and effectiveness of the proposed design method. It will be shown that in comparison with the analytical approach and genetic algorithms (GAs), the presented method can find both trivial and non-trivial flat-foldable solutions with considerably less effort and computational cost. Non-trivial flat-foldable patterns show different and interesting folding behaviors and enrich origami design.

Keywords: origami, flat-foldability, particle swarm optimization, graph theory, periodicity, folding, computational geometry, computational kinematics, computer-aided design, design automation, design optimization, kinematics, smart materials and structures

Introduction

An origami tessellation is a repetitive geometric design folded from a single sheet of paper [1]. While the vast majority of such designs are considered to be chiefly artistic, a number of them have been of special interest by the scientific community, enabling numerous applications in science and engineering such as deployable structures [2–7], biomedical devices [8–11], robotics [12–19], and metamaterials [20–25]. As a result, developing new origami tessellations and understanding their folding behaviors are important to enrich origami science and further promote their engineering applications.

To obtain a 3D shape with desired functionality or performance, origami designers generally focus on possible crease patterns on a 2D plane. This is because an appropriate arrangement of mountain and valley creases is the primary problem to be solved for obtaining the expected 3D shape [26]. Lang [27] has collected a series of mathematical and geometric techniques for origami design and developed systematic mathematical methods for designing new origami patterns [28]. Demaine and O'Rourke [29] proposed geometric folding algorithms for linkages and origami. Recent studies [30,31] have presented state-of-art reviews on the design methods, kinematic and mechanical analysis, and potential application of origami structures. On the basis of affine transformations and closed-loop equations, Belcastro and Hull introduced a matrix method to expound the continuous rotation of origami along the creases [32]. Starting from a single four-fold vertex in origami, Tachi [33] established a set of equations with boundary constraints for the edges and vertices and proposed a method for the generalization of quadrilateral mesh origami, which is both rigid and flat-foldable. Using input point sets in a Cartesian coordinate system, Zhou et al. [34] described a computational method to generate 3D origami structures with developability. Zirbel et al. [35] employed a mathematical model and hardware modifications to accommodate thickness in origami-based deployable arrays. To apply the origami concept for practical foldable structures, Chen et al. proposed a comprehensive kinematic synthesis for rigid origami of thick panels [36]. Using screw theory, Qiu et al. [37,38] verified that origami structures could be considered as equivalent redundantly actuated mechanisms. Then, by using closed-form screw-loop equations, Wei and Dai [39] obtained new origami folds and crease patterns from the evolved overconstrained mechanism. Recently, He and Guest [40] put forward a theoretical framework for rigid origami with straight-line creases. Zimmermann and Stanković [41] described a necessary and sufficient condition for the rigid foldability of a degree-4 vertex in origami patterns. Fuchi and Diaz [42] utilized the ground structure approach and a simple gradient-based search technique to find crease patterns of 2×2 origami tessellation.

In fact, well-known origami tessellations such as the Miura and Yoshimura patterns have been generalized by various researchers, with some generalized variations having global curvature when

[1]Corresponding author.

folded [26,43–45]. Through a systematic symmetry reduction process while maintaining the flat-foldability of each vertex, Johnson et al. [9] established a framework for generating symmetric derivatives of the Miura-ori and developed a large family of descendants for this classic tessellation. Based on graph theory, Chen et al. [46] developed an integrated geometric-graph-theoretic method to compactly represent origami tessellations using undirected and directed graph products. Further, it was demonstrated that this method can be utilized to enhance the configuration process and obtain involved matrices and origami models in an effective way. On the other hand, both flat-foldability (i.e., being transformable into a flat-folded state) and rigid foldability (i.e., being continuously foldable without any deformation of facets) are important constraints frequently applied to origami design. However, meeting the requirements for the satisfaction of these constraints is not straightforward in the design of many origami patterns [47,48]. Inspired by the development sequence through the ice-cracking process, McAdams and Li [49] introduced a genetic algorithm to design and optimize flat-foldable origami patterns. Although a range of origami design methods have been developed by mathematical or geometric approaches, designing origami tessellations faces considerable geometric or computational challenges. Numerical computational methods are preferred, which are expected to be robust and easy to implement. Besides, symmetry and regularity can be fully considered during origami design because most origami tessellations exhibit periodicity or regularity.

In this study, we propose a computational method for developing four-fold origami tessellations with flat-foldability. A key significance of this work is that the proposed method effectively combines a geometric-graph representation for the boundary conditions and a metaheuristic using particle swarm optimization (PSO). To solve the involved origami design problems with high computational complexity, interior four-fold vertices are taken as moving particles. Then, optimal positions of the vertices and possible distributions of crease lines are identified by the evolutionary computation using PSO. Next section reviews the basic theorems of four-fold origami patterns and presents flat-foldability constraints for the boundary vertices. Then, we present the optimization model for the involved origami design. In the section of Numerical Experiments, we provide several examples to verify the performance of the proposed design method.

Origami Tessellations With Four-Fold Vertices

Conditions for Local Flat-Foldability. There are three theorems governing the local flat-foldability of four-fold (i.e., degree-4) origami patterns, as given below:

THEOREM 1. *Assume a single-vertex fold pattern with four-fold crease lines identified by angles α_1, α_2, α_3, and α_4 so that $\alpha_1+\alpha_2+\alpha_3+\alpha_4=2\pi$ [29,50,51]. On the basis of the Kawasaki's theorem [29,51], the crease pattern is flat-foldable, if and only if the sum of the alternate angles around the vertex is π. That is*

$$\sum_{i=1}^{4}\alpha_i = 2\pi \quad \text{and} \quad \alpha_1+\alpha_3=\alpha_2+\alpha_4=\pi \tag{1}$$

This condition guarantees the local flat-foldability of each vertex in a multi-vertex pattern.

THEOREM 2. *The numbers of mountain and valley fold lines always differ by 2 [29,51], i.e.*

$$\begin{cases} n_m=3,\ n_v=1 & \text{if } n_m>n_v \\ n_m=1,\ n_v=3 & \text{otherwise} \end{cases} \tag{2}$$

where n_m and n_v denote the number of mountain and valley fold lines, respectively.

THEOREM 3. *An angle α_i which is strictly smaller than its two surrounding angles has two rays with opposite fold directions, i.e., one mountain and one valley fold line. In other words*

$$\{\alpha_i<\alpha_{i-1} \quad \text{and} \quad \alpha_i<\alpha_{i+1}\} \Rightarrow \alpha_i \tag{3}$$

is formed by one mountain and one valley fold lines.

Repetitive Flat-Foldable Patterns. Generated by the repetition of some finite sets of flat-foldable vertices, flat-foldable origami tessellations can be represented compactly in various mathematical forms. Figure 1 shows an example flat-foldable crease pattern derived from the conventional Miura-ori [44,52]. It is composed of 5×3 basic octagonal unit fragments (i.e., five units in the horizontal direction and three units in the vertical direction), where the horizontal lines in the original Miura-ori have been replaced by a set of zigzag polylines.

In fact, such a pattern can be exploited as an initial "geometric base" to numerically develop novel origami tessellations with displaced four-fold vertices, subject to the satisfaction of the local flat-foldability condition at each vertex of the new pattern. A previous study [46] has shown that based on graph theory, this pattern can be effectively expressed by the Cartesian product of graphs G_1 and G_2, i.e., $G_1 \square G_2$. In Fig. 1, the subgraphs G_1 and G_2 are two zigzag polylines. The horizontal zigzag polyline G_1 is expressed by two independent vectors $\boldsymbol{u}_1$ and $\boldsymbol{u}_2$ (originated from the nodes on the bottom left; see Fig. 1(*a*)). Similarly, the other zigzag

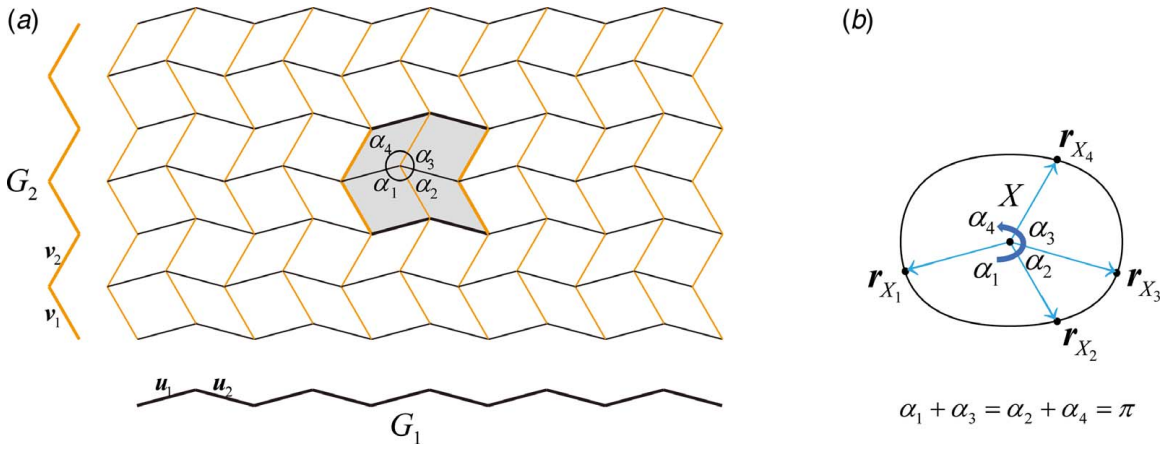

Fig. 1 A flat-foldable $pgg^{+}_{2,2}$ crease pattern with periodicity: (*a*) the pattern expressed by the Cartesian product of graphs G1 and G2, i.e., G1□G2 (the subgraphs G1 and G2 are two zigzag polylines) and (*b*) a typical four-fold vertex, X, of the unit fragment of the pattern

polyline G_2 is expressed by two vectors $\boldsymbol{v}_1$ and $\boldsymbol{v}_2$. Moreover, θ_{u1}, θ_{u2}, θ_{v1}, and θ_{v2} denote the angles between respective vectors and the x-axis ($\theta \in (-\pi, \pi)$; positive angles are counterclockwise), and $|\boldsymbol{u}_1|$, $|\boldsymbol{u}_2|$, $|\boldsymbol{v}_1|$, and $|\boldsymbol{v}_2|$ represent the lengths of respective edges. For instance, in Fig. 1(*a*), $\theta_{u1} = \pi/12$, $\theta_{u2} = -\pi/12$, $\theta_{v1} = 2\pi/3$, $\theta_{v2} = \pi/3$, and each edge has a unit length.

Flat-Foldability of a Generic Four-Fold Vertex. Figure 1(*b*) shows the flat-foldability in terms of the alternate angles around a typical four-fold vertex, X, of the unit fragment of the pattern. In this figure, $\boldsymbol{r}_{X_i}$ denotes the unit vector originating from vertex X along the ith fold line and can be expressed as

$$\boldsymbol{r}_{X_i} = \frac{\mathbf{XX_i}}{|\mathbf{XX_i}|} \tag{4}$$

where the integer i can be taken as 1, 2, 3, or 4 and X_i represents one of the four nodes surrounding vertex X. Then, Eq. (1) can be expressed by the following vector notation:

$$\begin{aligned}\cos^{-1}(\boldsymbol{r}_{X_1} \cdot \boldsymbol{r}_{X_2}) + \cos^{-1}(\boldsymbol{r}_{X_3} \cdot \boldsymbol{r}_{X_4}) = \cos^{-1}(\boldsymbol{r}_{X_2} \cdot \boldsymbol{r}_{X_3}) \\ + \cos^{-1}(\boldsymbol{r}_{X_4} \cdot \boldsymbol{r}_{X_1}) = \pi\end{aligned} \tag{5}$$

which is the governing equation for the flat-foldability of a four-fold vertex.

As shown in Fig. 2(*a*), the octagonal unit fragment associated with a $pgg^{+}_{2,2}$ derivative [44,53] of the Miura pattern contains four independent four-fold vertices: node N_1 (equivalently nodes N_3, N_7, and N_9), node N_2 (equivalently node N_8), node N_4 (equivalently node N_6), and node N_5. Based on graph theory and periodic symmetry [54,55], the positions of all the vertices can be efficiently evaluated. For example, the position of an inner vertex $\boldsymbol{X}_{N_5}^{(m-n)}$ is given by

$$\boldsymbol{X}_{N_5}^{(m-n)} = \boldsymbol{X}_{N_5}^{(1-1)} + (m-1)(\boldsymbol{u}_1 + \boldsymbol{u}_2) + (n-1)(\boldsymbol{v}_1 + \boldsymbol{v}_2) \tag{6}$$

where m and n denote the order number of the unit fragment along the horizontal and vertical directions, respectively, and $\boldsymbol{X}_{N_5}^{(1-1)} = \boldsymbol{X}_{N_5}$ represents the nodal coordinates of vertex N_5.

Importantly, the unit fragment of an origami tessellation with four-fold vertices is not necessarily octagonal [54,55]. To deal with design problems involving polygons with complex boundaries, we propose a metaheuristic design generation method which is not limited to octagonal unit fragments but can be also generalized for more complex unit fragments. Without loss of generality, a given unit fragment can be expressed by the Cartesian product, $G_1 \square G_2$, of two independent subgraphs G_1 and G_2. As illustrated in Fig. 2(*b*), the subgraph G_1 contains a matrix of independent vectors $\mathbf{U} = [\boldsymbol{u}_1, \boldsymbol{u}_2, \ldots, \boldsymbol{u}_{\text{end}}]$, and the subgraph G_2 contains a matrix of independent vectors $\mathbf{V} = [\boldsymbol{v}_1, \boldsymbol{v}_2, \ldots, \boldsymbol{v}_{\text{end}}]$; here $\boldsymbol{u}_{\text{end}}$ and $\boldsymbol{v}_{\text{end}}$ denote the last vectors—terminated at the end nodes of the subgraphs G_1 and G_2, respectively. Whilst the boundary nodes are fully determined by these matrices of independent vectors, the internal four-fold nodes still need to be determined. In addition, the connectivity pattern of vertices of the unit fragment can be obtained from the adjacency matrix of the Cartesian product $G_1 \square G_2$ of the graphs G_1 and G_2. Then, according to the periodicity of the pattern and by using Eq. (6), the nodal vector $\boldsymbol{X}$ of each vertex of the obtained origami pattern can be given by

$$\boldsymbol{X}^{(m-n)} = \boldsymbol{X}^{(1-1)} + (m-1)\sum_{i \in G_1} \boldsymbol{u}_i + (n-1)\sum_{j \in G_2} \boldsymbol{v}_j \tag{7}$$

The local flat-foldability of "corner" boundary nodes—shared by four unit fragments—should be first considered (i.e., node N_1 (equivalently nodes N_3, N_7, and N_9), shown in Fig. 2(*a*)). Hence, we establish a constraint for the initial geometry of the subgraphs, where the first and end vectors of the given unit fragment should satisfy

$$\theta_{u_1} + \theta_{u_{\text{end}}} = \theta_{v_1} + \theta_{v_{\text{end}}} - \pi \tag{8}$$

where $\theta_{u_{\text{end}}} \in (-\pi, \pi)$ denotes the angle between the end vector $\boldsymbol{u}_{\text{end}}$ and the x-axis (positive angles are counterclockwise), and $\theta_{v_{\text{end}}} \in (-\pi, \pi)$ denotes the angle between the end vector $\boldsymbol{v}_{\text{end}}$ and the x-axis (e.g., the angle θ_{v2} shown in Fig. 2(*a*)). Note that, when the given unit fragment is an octagon, Eq. (8) is equivalent to the presented constraint for the internal angles at nodes N_1 and N_3 [44,56]. Then, in order to develop a flat-foldable origami tessellation, the flat-foldability condition at the internal nodes and the boundary nodes shared by two unit fragments (e.g., nodes N_2, N_4, N_6, and N_8, shown in Fig. 2(*a*)) should be also satisfied. Finally, when each vertex satisfies the local flat-foldability condition, the folding sequence of the origami structure can be simulated to verify the global flat-foldability by certain folding methods [3,57].

Optimization Framework. In general, as the number of nodes of a tessellation increases, it progressively becomes difficult to analytically compute the complete solution where the flat-foldability conditions at all vertices are satisfied simultaneously [47]. Here, we adopt an optimization framework to solve such problems. Based on Eqs. (1) and (5), an error function $e(\boldsymbol{X})$ for evaluating the local flat-foldability of a typical vertex X is defined as follows:

$$e(\boldsymbol{X}) = |\cos^{-1}(\boldsymbol{r}_{X_1} \cdot \boldsymbol{r}_{X_2}) + \cos^{-1}(\boldsymbol{r}_{X_3} \cdot \boldsymbol{r}_{X_4}) - \pi| \tag{9}$$

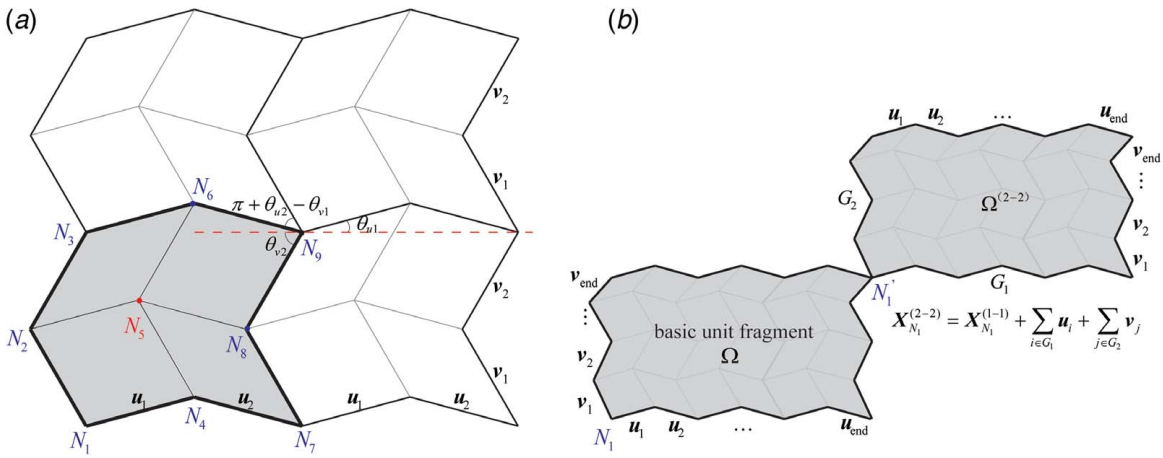

Fig. 2 Local flat-foldability of typical four-fold vertices within: (*a*) an octagonal unit and (*b*) two diagonally connected, polygonal unit fragments

where $e(\boldsymbol{X}) \in [0, \pi]$ and $e(\boldsymbol{X}) = 0$, if the vertex satisfies the local flat-foldability condition. To satisfy the flat-foldability condition at all vertices, the total error for different types of nodes (e.g., internal nodes, boundary nodes shared by two unit fragments, and corner nodes shared by four unit fragments) should be minimized and ideally "zero."

As can be seen from Fig. 2, the position of an internal node affects both the geometry of the origami pattern and the flat-foldability at the boundary nodes. In this case, the positions of the internal nodes within the given unit fragment are taken as design variables. Thus, the optimization model for generating flat-foldable origami patterns can be expressed as

$$\begin{array}{ll} \text{minimize} & f = \sum e(\boldsymbol{X}) \\ \text{subject to} & \boldsymbol{X} \subset \Omega \end{array} \tag{10}$$

In Eq. (10), Ω denotes the closed planar region within the basic unit fragment, which is determined by the given matrices $\mathbf{U} = [\boldsymbol{u}_1, \boldsymbol{u}_2, \ldots, \boldsymbol{u}_{\text{end}}]$ and $\mathbf{V} = [\boldsymbol{v}_1, \boldsymbol{v}_2, \ldots, \boldsymbol{v}_{\text{end}}]$. The optimization algorithm is expected to search for different optimal points starting from the initial positions of the internal nodes. However, the boundary constraint in Eq. (10) is too strong for the optimization process to converge. Some obtained points can either go beyond the boundary (i.e., $\boldsymbol{X} \not\subset \Omega$) or generate self-intersecting crease lines. To avoid self-intersecting and out-of-range results, the concept of the algebraic area is utilized [47]. For instance, the area of a general quadrilateral facet *ABCD* is

$$S = 0.5|(\boldsymbol{X}_C - \boldsymbol{X}_A) \times (\boldsymbol{X}_D - \boldsymbol{X}_B)| \tag{11}$$

where the illustrative vertices *A*, *B*, *C*, *D* of the quadrilateral can be numbered in a clockwise or counterclockwise direction. Mathematically, on condition that each vertex $\boldsymbol{X} \subset \Omega$, the sum of the areas of all the quadrilateral facets without self-intersection is necessarily equal to the area of the given unit fragment, i.e.

$$S_{\text{UF}} = \sum S \tag{12}$$

Based on Eq. (12) and the concept of penalty, an error function $e_S(\boldsymbol{X})$ is introduced for evaluating facets of the quadrilaterals formed by the four-fold vertices

$$e_S(\boldsymbol{X}) = \frac{\left|S_{\text{UF}} - \sum S\right|}{\left|S_{\text{UF}} - \sum S\right| + 1} \tag{13}$$

where $e_S(\boldsymbol{X}) \in [0, 1)$. Furthermore, to develop physically fabricatable origami patterns, the following constraint for the lengths of the fold lines is added to the optimization process:

$$e_L(\boldsymbol{X}) = \begin{cases} 0, & \text{if } \eta_{\min} l_{\min} < |\mathbf{XX_i}| < \eta_{\max} l_{\max} \\ \pi, & \text{otherwise} \end{cases} \tag{14}$$

where $l_{\min}$ and $l_{\max}$ are, respectively, the minimum and maximum lengths of the boundary edge lines, and $\eta_{\min}$ and $\eta_{\max}$ are the lower and upper multiplication factors (in this study, $\eta_{\min} = 0.2$ and $\eta_{\max} = 4$). Hence, based on Eqs. (10), (13), and (14), the objective function is modified as follows to effectively produce optimal solutions:

$$\text{minimize} \quad f = e_L(\boldsymbol{X}) + e_S(\boldsymbol{X}) + \sum e(\boldsymbol{X}) \tag{15}$$

When every four-fold vertex satisfies the flat-foldability condition and the objective function *f* gets sufficiently close to zero (in this study, $f < 10^{-6}$), an optimized, flat-foldable origami pattern will be obtained.

On the other hand, it is important to point out that the PSO is a robust computational method searching a population of candidate solutions within very large solution spaces, which is inspired by the movement of organisms in a bird flock or fish school [58]. Because of few or no assumptions needed for the involved problem, PSO is one of the most widely applied metaheuristic algorithms [59]. It does not require the optimization problem to be differentiable, which is generally required by classic optimization methods (such as the quasi-newton and gradient descent methods). PSO is originally attributed to Kennedy and Eberhart [60] and gets successful applications in the design of four-bar mechanisms [61], force-finding of cable-strut structures [62], topology optimization of truss structures [62], etc. Here, we adopt the PSO for solving the above-mentioned optimization problem for flat-foldable origami patterns in order to effectively and iteratively move a large number of candidate solutions toward the best solution in the search-space.

During the evolutionary computation using PSO, n_s denotes the number of particles. First, each particle is initialized to randomly distribute in the search-space, with position $\boldsymbol{x}_i \subset \Omega$ and velocity $v_i \in [0, v_{\max}]$, where $v_{\max}$ is the maximum velocity of the particles. The local-best position of a particle is denoted by $\boldsymbol{p}_i$, and the global-best position of all the particles is denoted by $\boldsymbol{g}$. The velocity of each particle is iteratively updated by

$$\begin{aligned} v_i = \omega \cdot v_i + c_1 \cdot \text{rand}(0,\ 1) \cdot (\boldsymbol{p}_i - \boldsymbol{x}_i) \\ + c_2 \cdot \text{rand}(0,\ 1) \cdot (\boldsymbol{g} - \boldsymbol{x}_i), \quad \text{and} \quad v_i \in [0, v_{\max}] \end{aligned} \tag{16}$$

where c_1 and c_2 are the acceleration constants and rand (0, 1) denotes a random value in the range [0,1]. In Eq. (16), ω is the inertia weight for enhancing the global searching capability, which can be determined by the linearly decreasing weight. In other words, at iteration step *t*, the inertia weight ω is given by

$$\omega^t = (\omega_{\text{initial}} - \omega_{\text{end}}) \cdot (t_{\max} - t)/t_{\max} + \omega_{\text{end}} \tag{17}$$

where ω_{initial} and ω_{end} denote the decreasing weight at the initial step and the end step, respectively. Subsequently, the position of particle *i* is updated by

$$\boldsymbol{x}_i = \boldsymbol{x}_i + v_i \tag{18}$$

Then, the local-best position of particle *i* is updated by

$$\boldsymbol{p}_i = \boldsymbol{x}_i, \quad \text{if} \quad f(\boldsymbol{x}_i) < f(\boldsymbol{p}_i) \tag{19}$$

and the global-best position of all the particles is updated by

$$\boldsymbol{g} = \boldsymbol{p}_i, \quad \text{if} \quad f(\boldsymbol{p}_i) < f(\boldsymbol{g}) \tag{20}$$

As a result, based on Eqs. (16)–(20), each particle keeps moving toward the optimal position and $t = t + 1$. Note that the iteration should be terminated when optimal solutions are obtained or the step $t = t_{\max}$. The proposed design generation process has been implemented in MATLAB, where the flowchart of the PSO-based design process is given in Fig. 3.

Numerical Experiments

In this section, several numerical examples are presented to verify the performance of the proposed method for generating origami patterns. All the examples have been implemented in MATLAB. The number of particles is $n_s = 400$. The maximum velocity of the particles in Eq. (16) is denoted as $v_{\max} = 0.2L_{\min}$, and $L_{\min}$ is the shorter one between the full width and height of the given unit fragment. The parameters in Eqs. (16) and (17) are chosen as $w_{\text{initial}} = 0.2$, $w_{\text{end}} = 0.9$, $c_1 = c_2 = 2$, and $t_{\max} = 1000$. These parameters have been carefully determined to control the behavior and efficacy of the PSO method [59,62].

Flat-Foldable Tessellations for a Given Octagonal Unit Fragment (Single Design Variable). To verify the feasibility of the proposed method, we start with a simple and well-known octagonal unit fragment [56]. Based on the given positions of the boundary nodes of the octagonal unit fragment, the

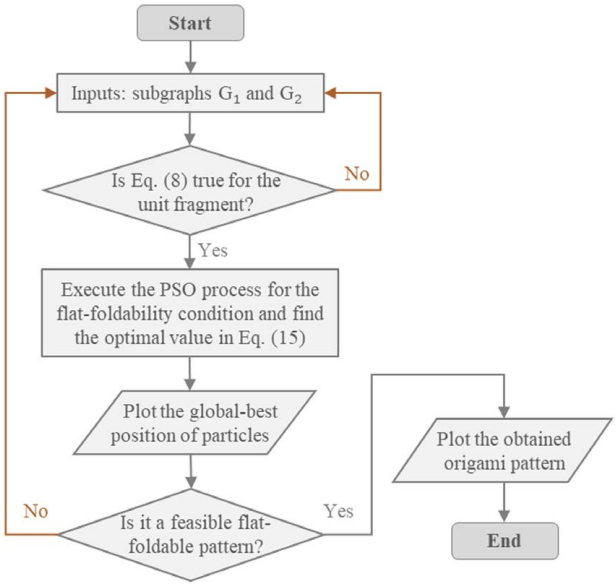

Fig. 3 Flowchart of the PSO-based design generation process of the four-fold origami tessellation

specifications of vectors describing the basic unit fragment are expressed as follows:

$$|\boldsymbol{u}_1| = 0.985|\boldsymbol{v}_2|, \quad |\boldsymbol{u}_2| = 0.685|\boldsymbol{v}_2|, \quad |\boldsymbol{v}_1| = 0.655|\boldsymbol{v}_2|,$$
$$\theta_{u1} = 0, \quad \theta_{u2} = -\pi/9, \quad \theta_{v1} = 2\pi/9, \quad \text{and} \ \ \theta_{v2} = 2\pi/3 \tag{21}$$

Then, based on the given boundary, the proposed method is utilized to find optimal solutions multiple times, each time using variables randomly distributed within the octagonal unit fragment. Because of symmetry, all possible tessellations can be formed from the obtained pattern of the octagonal unit fragment. Two different solutions were found by the proposed method within 200 steps. Figure 4 illustrates the flat-foldable tessellations (represented by 2×2 unit fragments) corresponding to the two solutions.

As can be seen from Fig. 4(*a*), the first feasible pattern is a $(p2)^{+}_{2,2}$ derivative [47] of the Miura-ori, where the internal fold lines are parallel to the borderlines of the octagonal unit fragment. As the initial parameters denoted in Eq. (21) to meet the constraints for the subgraphs (i.e., $\theta_{u_1} + \theta_{u_2} = \theta_{v_1} + \theta_{v_2} - \pi$), each vertex satisfies the flat-foldability condition. More importantly, as shown in Fig. 4(*b*), a non-obvious flat-foldable pattern is developed. This pattern consists of four different convex quadrilateral facets, and the angles at the four-fold vertices are different. Although there is no parallelogram in the obtained pattern, each vertex strictly satisfies the flat-foldability condition. Notably, both of the obtained patterns are valid, as they are in good agreements with those tessellating variations of the Miura-ori presented by Sareh [44] and Sareh and Guest [56] using the analytic approach.

Figure 5 illustrates the convergence histories associated with the two solutions presented in Fig. 4, demonstrating the substantial reduction of the function value and the swarm motion of particles within the unit fragment. In less than 180 iterations, the PSO algorithm can find the two solutions.

It turns out that the computational cost for obtaining the trivial solution is slightly lower than that of the non-trivial solution. As shown in Fig. 5, at initial iteration steps, a small number of particles move far from the feasible solutions and even go beyond the boundary constraints. Nevertheless, a swarm of particles approaches an optimal solution within 110 iteration steps. Subsequently, more and more particles move toward them and gather around the optimal solution. Therefore, the proposed method shows global and excellent convergence.

Using the proposed method, we can find out the geometry and the sector angles of each vertex. Regarding the mountain-valley folds assignment, the obtained geometry should be further checked based on the flat-foldable conditions and the folding methods [3,57]. For instance, Fig. 6 shows 6×6 origami tessellations corresponding to the two obtained solutions. Observing the fully folded configurations shown in Figs. 6(*a*) and 6(*b*), we conclude that both origami patterns are flat-foldable. The complete configuration of the generalized Miura pattern remains in a planar state during folding. On the contrary, the novel pattern exhibits a remarkable shape-changing, where the radius of curvature of the structure reduces significantly during folding. In other words, although the initial octagonal unit fragment and its topology keep unchanged, the patterns corresponding to the trivial and non-trivial solutions exhibit completely different folding configurations and kinematic behavior. Thus, finding non-trivial solutions of a given fragment is important for enriching origami design and provides potential applications of origami structures with transformable configurations and folding behavior.

It is important to point out that our PSO-based method is applicable to arbitrary octagonal unit fragments. For example, given

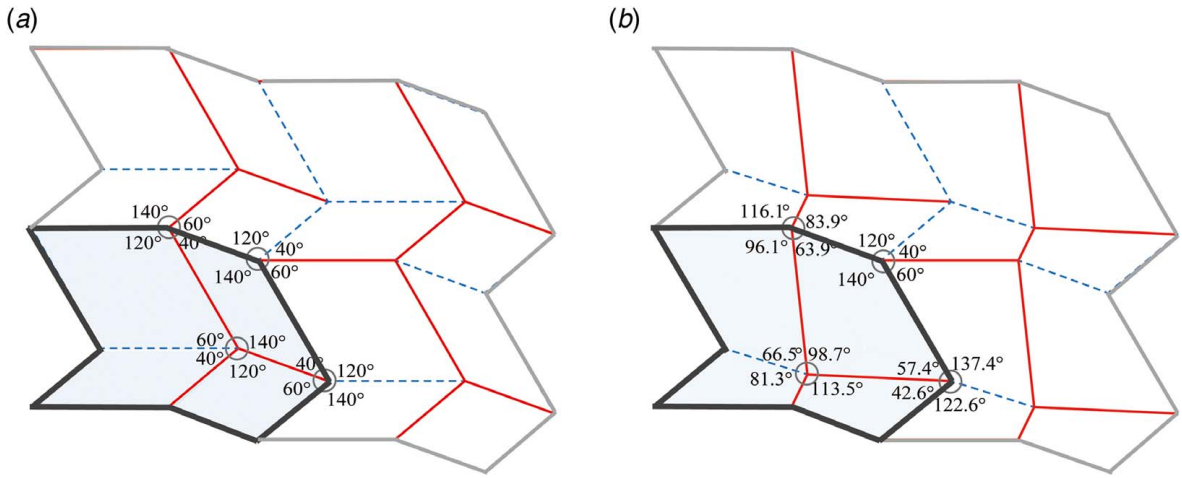

Fig. 4 Origami patterns with two different positions of four-fold vertices: (*a*) the trivial $(p2)^{+}_{2,2}$ derivative of the Miura-ori and (*b*) the non-trivial $(p1)_{2,2}$ derivative of the Miura-ori [47] (solid and dashed lines represent mountain and valley folds, respectively; bold black lines represent the octagonal unit fragment of each pattern)

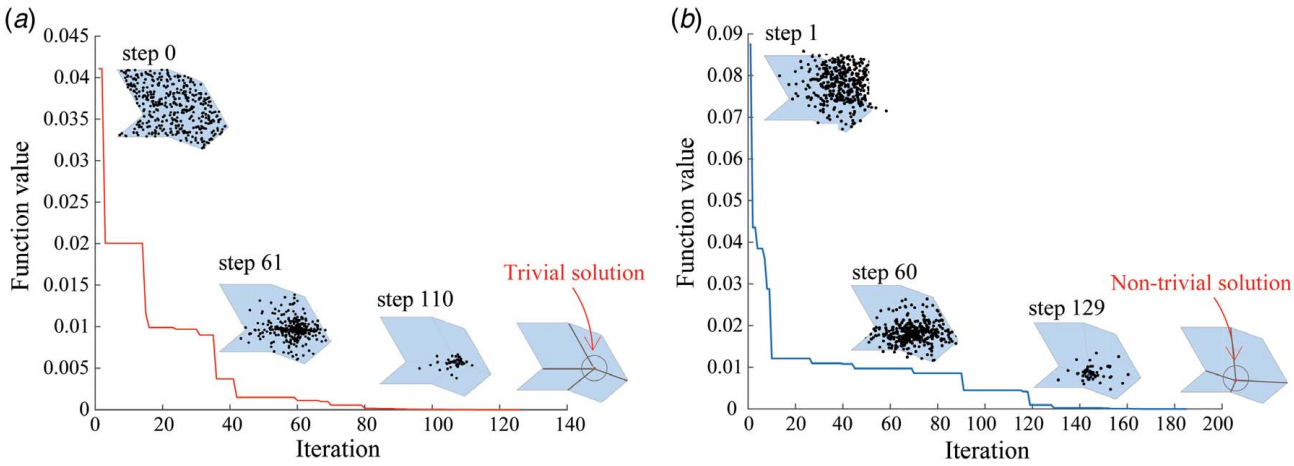

Fig. 5 Iteration histories and typical distributions of particles during the optimization processes: (*a*) the trivial $(p2)^{+}_{2,2}$ derivative of the Miura-ori and (*b*) the non-trivial $(p1)_{2,2}$ derivative of the Miura-ori

another octagonal unit, the specifications of the vectors describing the subgraphs are as follows

$$|\boldsymbol{u}_1|=0.5|\boldsymbol{v}_2|,\quad |\boldsymbol{u}_2|=|\boldsymbol{v}_2|,\quad |\boldsymbol{v}_1|=0.8|\boldsymbol{v}_2|,\quad \theta_{u1}=0,\\ \theta_{u2}=\pi/18,\quad \theta_{v1}=23\pi/36,\quad \text{and}\ \ \theta_{v2}=5\pi/12 \tag{22}$$

Using the PSO-based method and the geometry denoted in Eq. (22), we can develop two flat-foldable origami patterns. The results are shown in Fig. 7, where the angles at the four typical four-fold vertices *A*, *B*, *C*, and *D* are evaluated and listed in Table 1.

To further explore the computational efficiency, the proposed method is compared with other existing metaheuristic algorithms such as the genetic algorithm (GA). The whole process is implemented in the optimization toolbox GA in MATLAB, where the optimization model keeps invariant. The iteration history of the PSO and GA methods for optimizing the two patterns is also shown in Fig. 7.

As can be seen from Fig. 7, in comparison with the GA method, the proposed PSO algorithm achieves better results with higher convergence rates. There are no crossover or mutation operations in PSO, which is a key process for GA. All particles are continuously updated by the current velocities and foraging behavior of the swarm of particles. Hence, the principle behind PSO is substantially simpler. Moreover, the PSO method requires significantly fewer parameters, making it is easier to implement.

On the other hand, many feasible solutions can be simultaneously obtained by the PSO method. For example, the octagonal unit

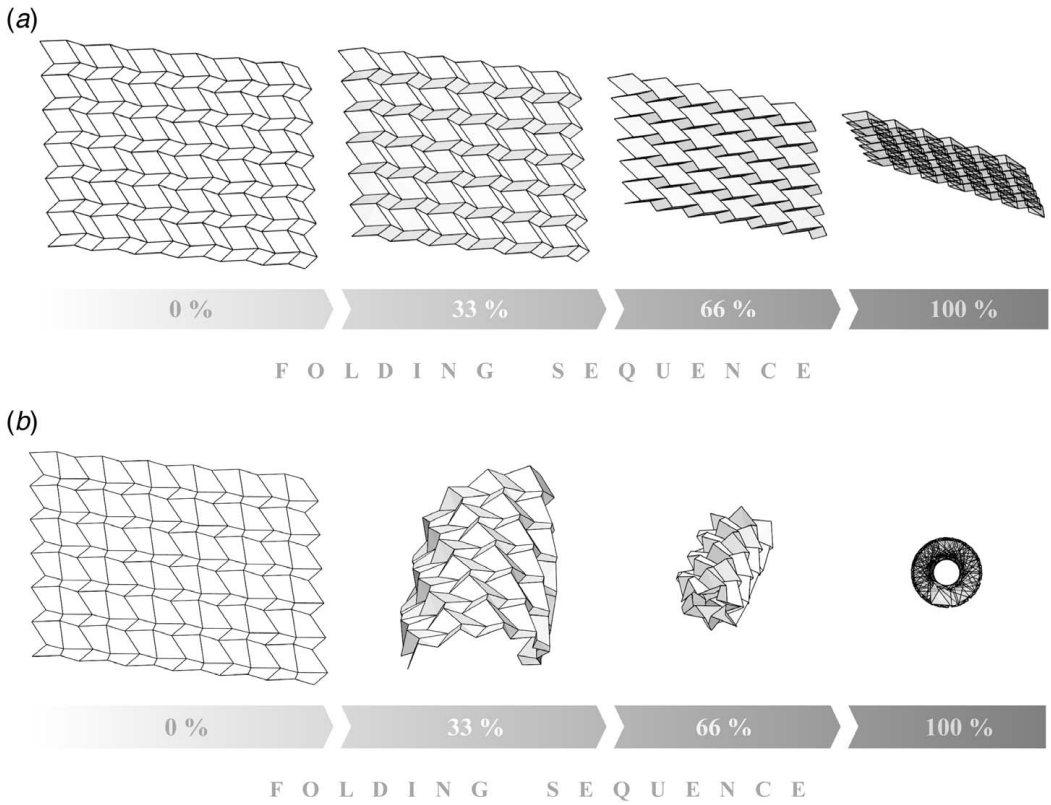

Fig. 6 Folding sequence of origami tessellations consisting of 6 × 6 octagonal unit fragments: (*a*) the trivial $(p2)^{+}_{2,2}$ and (*b*) the non-trivial $(p1)_{2,2}$, derivatives of the Miura-ori

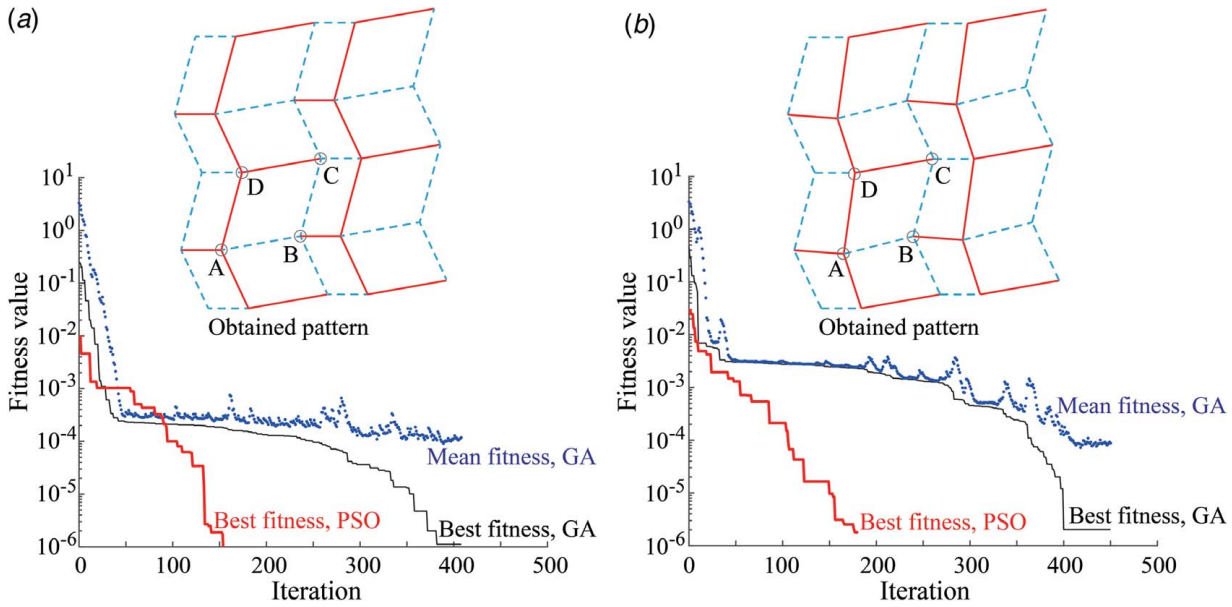

Fig. 7 Iteration history of PSO and GA for optimizing: (*a*) the expected pattern corresponding to the trivial solution and (*b*) a novel pattern corresponding to the non-trivial solution

Table 1 Angles α_1, α_2, α_3, and α_4 evaluated at the respective vertices of the two patterns

	Trivial pattern in Fig. 7(*a*)				Non-trivial pattern in Fig. 7(*b*)			
Vertex	A	B	C	D	A	B	C	D
α_1	115.00 deg	105.00 deg	65.00 deg	75.00 deg	112.08 deg	100.79 deg	65.00 deg	82.14 deg
α_2	75.00 deg	65.00 deg	105.00 deg	115.00 deg	86.35 deg	60.79 deg	105.00 deg	107.86 deg
α_3	65.00 deg	75.00 deg	115.00 deg	105.00 deg	67.92 deg	79.21 deg	115.00 deg	97.86 deg
α_4	105.00 deg	115.00 deg	75.00 deg	65.00 deg	93.65 deg	119.21 deg	75.00 deg	72.14 deg

fragment associated with a classic Miura fold pattern is chosen as a case to study, where the vectors corresponding to the subgraphs are specified by

$$|\boldsymbol{u}_1| = |\boldsymbol{u}_2| = |\boldsymbol{v}_1| = |\boldsymbol{v}_2|, \quad \theta_{u1} = \theta_{u2} = 0, \quad \theta_{v1} = 23\pi/36, \quad \text{and} \ \ \theta_{v2} = \pi - \theta_{v1} \tag{23}$$

With these given parameters, the proposed method is utilized to find feasible solutions. Figure 8 graphically shows the distribution trends of swarm particles. Some feasible solutions are found after 120 iteration steps, whereas many particles are accumulated along the horizontal symmetry axis. When the iteration process ends, a series of feasible solutions are detected to be distributed along the symmetry axis. Due to the reflectional symmetry, the four angles associated with every vertex on the symmetry axis necessarily satisfy

$$\alpha_1 = \alpha_4, \ \alpha_2 = \alpha_3 \quad \text{and} \ \ \alpha_1 + \alpha_3 = \alpha_2 + \alpha_4 = \alpha_1 + \alpha_2 = \pi \tag{24}$$

Consequently, each vertex on the symmetry axis is proven to be a feasible solution to the flat-foldability equation, verifying the theoretical results.

Flat-Foldable Tessellations for a Given Polygonal Unit Fragment (Multiple Design Variables). The proposed method is not limited to developing origami patterns for octagonal unit fragments, but the design variables may contain multiple four-fold vertices moving within a predetermined polygonal boundary. For

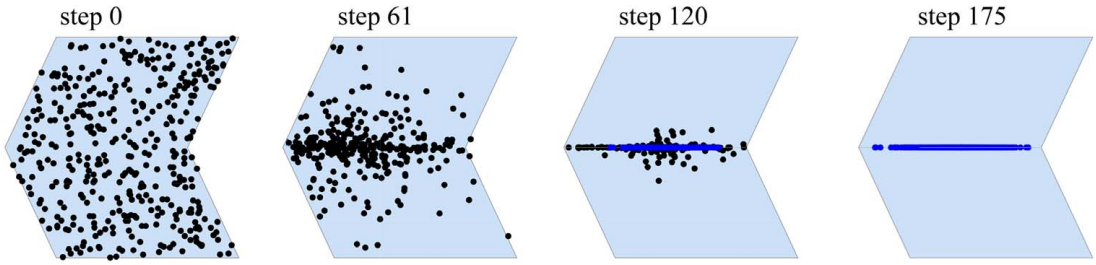

Fig. 8 Many feasible solutions for generalized Miura patterns obtained by PSO

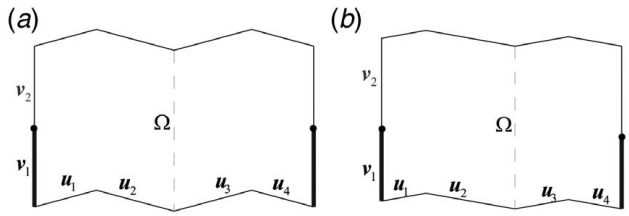

Fig. 9 Predetermined boundaries with 12 given nodes and multiple design variables: (*a*) a symmetric pattern and (*b*) an asymmetric pattern

example, Fig. 9 shows two predetermined boundaries with and without symmetry. Each boundary can be obtained by combining two octagonal units and consists of 12 boundary nodes and three internal nodes.

In fact, the subgraphs for describing the symmetric unit cell shown in Fig. 9(*a*) are given by

$$\begin{aligned} &|\boldsymbol{u}_1| = |\boldsymbol{u}_4| = 0.8|\boldsymbol{v}_2|, \quad |\boldsymbol{u}_2| = |\boldsymbol{u}_3| = |\boldsymbol{v}_2|, \quad |\boldsymbol{v}_1| = |\boldsymbol{v}_2|, \\ &\theta_{u1} = \theta_{u3} = \pi/12, \quad \theta_{u2} = \theta_{u4} = -\pi/12, \quad \text{and} \\ &\theta_{v1} = \theta_{v2} = \pi/2 \end{aligned} \tag{25}$$

Similarly, the subgraphs for describing the asymmetric unit cell shown in Fig. 9(*b*) are expressed as

$$\begin{aligned} &|\boldsymbol{u}_1| = 0.5|\boldsymbol{v}_2|, \quad |\boldsymbol{u}_2| = |\boldsymbol{v}_2|, \quad |\boldsymbol{u}_3| = |\boldsymbol{u}_4| = 0.6|\boldsymbol{v}_2|, \quad |\boldsymbol{v}_1| = 0.8|\boldsymbol{v}_2|, \\ &\theta_{u1} = \theta_{u3} = \pi/18, \quad \theta_{u2} = \theta_{u4} = -\pi/18, \quad \text{and} \\ &\theta_{v1} = \theta_{v2} = \pi/2 \end{aligned} \tag{26}$$

Using the proposed PSO method and the above-mentioned parameters, we can effectively generate a series of flat-foldable origami patterns. Typical configurations obtained from Figs. 9(*a*) and 9(*b*) are shown in Figs. 10(*a*)–10(*f*), respectively. As multiple four-fold vertices can move within the given region shown in Fig. 9, there are a series of feasible solutions to the optimization model. However, it becomes much difficult to obtain solutions for the irregular boundary. We validate that it is considerably easier for the proposed method to converge for the symmetric pattern in comparison with the asymmetric pattern. As the given fragment shown in Fig. 9(*a*) retains mirror symmetry, one of the internal nodes is always located on the symmetry axis. Then, the obtained origami patterns are likely to keep mirror symmetry, as verified by Figs. 10(*a*)–10(*c*).

Computer simulations based on nonlinear folding methods [63] are employed to verify the continuous folding behavior of these origami tessellations. For instance, Fig. 11 illustrates the folding sequence of the symmetric and asymmetric origami tessellations, represented by 4×3 arrays of unit cells, as shown in Figs. 10(*b*) and 10(*e*), respectively. Numerical simulations verify that each of the above-mentioned origami patterns is flat-foldable, rigid foldable, and retains a single-degree-of-freedom. Interestingly, as shown in Fig. 11(*b*), the asymmetric pattern shown in Fig. 10(*e*) has a significant global curvature.

To further evaluate the effectiveness of the proposed method, the results are compared with those using the GA algorithm. Figure 12(*a*) shows the iteration history of the PSO and GA methods for developing symmetric origami patterns shown in Fig. 9(*a*), while Fig. 12(*b*) shows the iteration history of both methods for developing asymmetric patterns shown in Fig. 9(*b*). Moreover, Fig. 12(*c*) shows the variations of the fitness value using the PSO-based optimization models with different parameters. The number of particles is taken as $n_s = 200$, 400, and 800, and the maximum velocity of the particles is $v_{\max} = 0.04L_{\min}$, $0.2L_{\min}$, and $L_{\min}$, respectively.

Figures 12(*a*) and 12(*b*) show that both GA and PSO methods can get satisfactory solutions to generate flat-foldable origami patterns in less than 700 steps, whereas asymmetric patterns require slightly more steps than symmetric patterns. The GA method has a relatively stable iteration process, as the mean fitness reflects the ability to converge. Notably, the proposed PSO method has a stronger convergence ability after 300 iteration steps. Moreover, the PSO method has more satisfactory computational accuracy than the GA method because the best fitness value f of the PSO method is far less than that of the GA method.

It can be noticed from Fig. 12(*c*) that the number n_s slightly affects the results, whereas more particles lead to the stronger capability of convergence. 400 particles are enough to obtain the optimal solutions. However, $n_s < 200$ particles frequently result in local optimal solutions (not feasible origami patterns). In addition, Fig. 12(*c*) shows that the convergence performance of the proposed method is slightly dependent on the maximum velocity of the particles $v_{\max}$, which should be set within a reasonable range. The particles with very small velocities ($v \ll 0.2L_{\min}$) lead to slower convergence, while the particles with fast motions are easy to get cross the optimal solution.

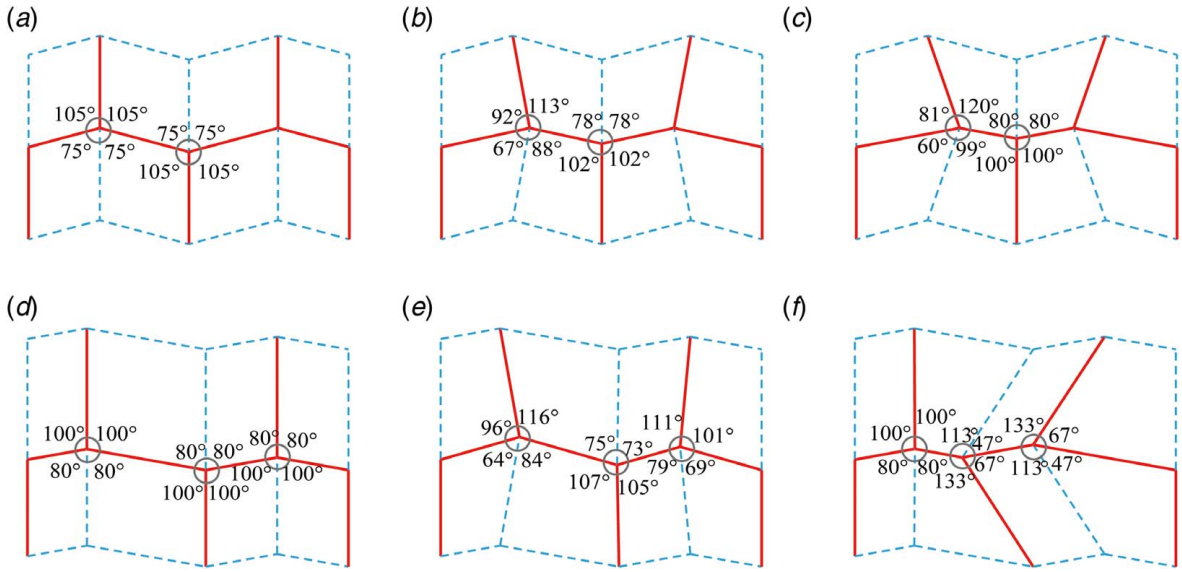

Fig. 10 Typical computationally generated flat-foldable patterns for a predetermined boundary: (*a*)–(*c*) symmetric patterns and (*d*)–(*f*) asymmetric patterns

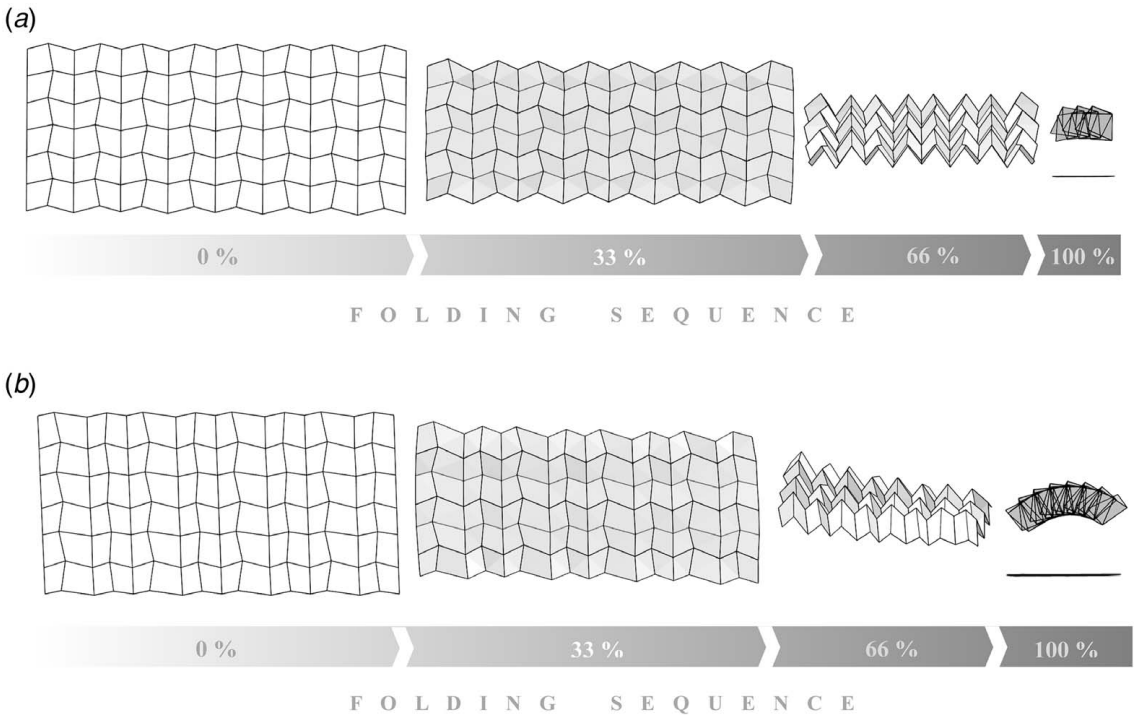

Fig. 11 Flat-folding sequences of origami tessellations composed of 4×3 unit fragments: (*a*) the symmetric pattern shown in Fig. 10(*b*) and (*b*) the asymmetric pattern shown in Fig. 10(e)

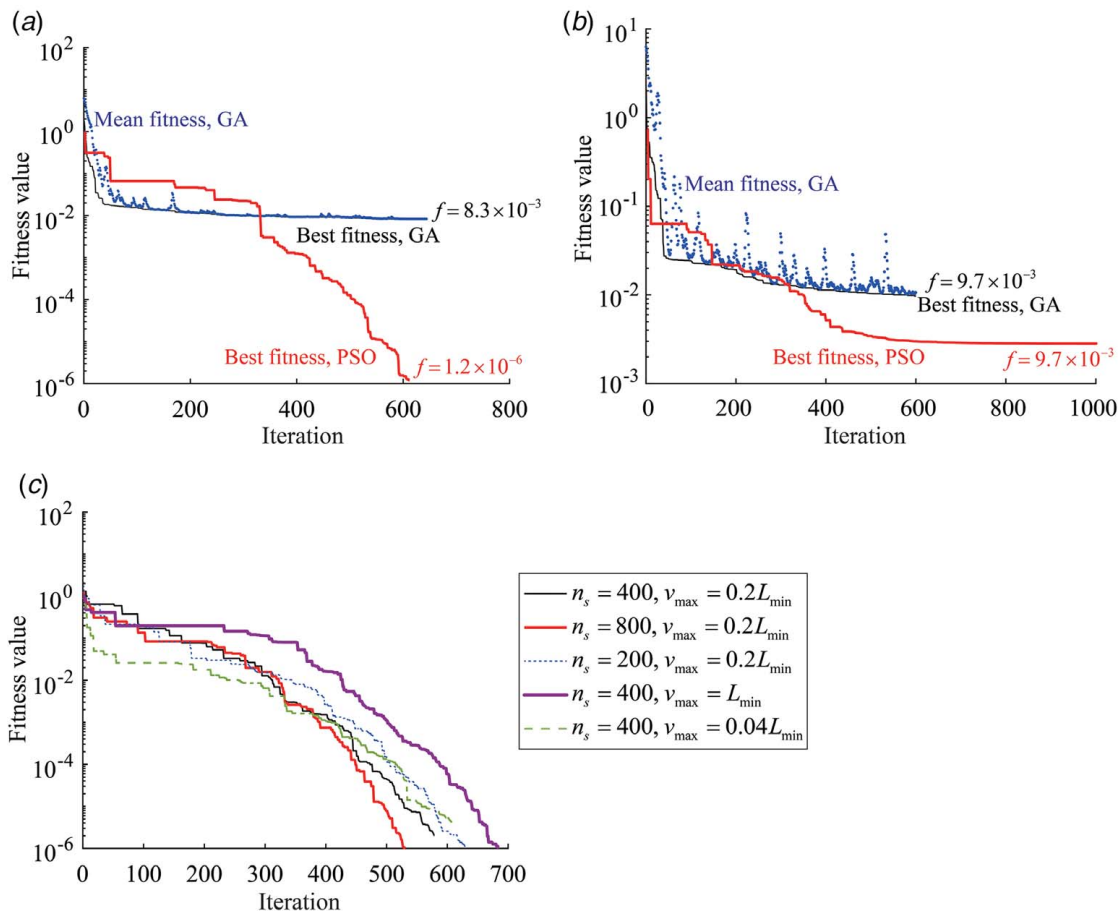

Fig. 12 Iteration history for developing non-trivial origami patterns: (*a*) PSO and GA methods for the symmetric pattern, (*b*) PSO and GA methods for the asymmetric pattern, and (*c*) the PSO method with different parameters

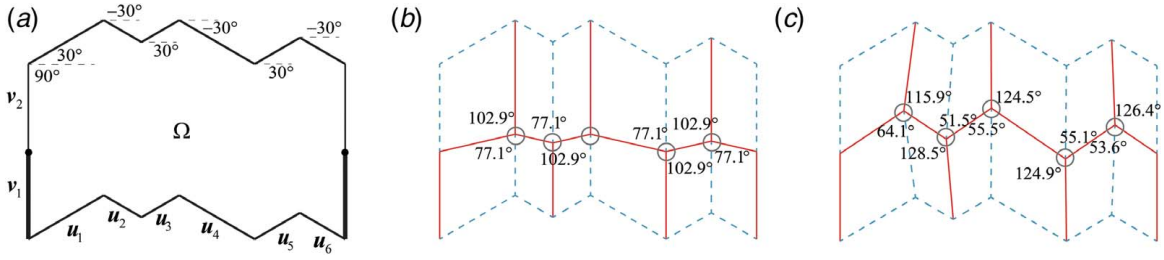

Fig. 13 A predetermined boundary with a vertical path graph: (*a*) geometry and (*b* and *c*) feasible origami patterns

Flat-Foldable Tessellations for a Given Complex Unit Fragment With 16 Boundary Nodes and Five Internal Nodes. To further evaluate the effectiveness of the proposed method for complex boundary geometries, two different unit fragments with 21 four-fold vertices are studied in this section. Each problem involves ten independent design variables. Figure 13(*a*) shows a unit fragment with regular boundary, whereas the subgraph G_1 contains zigzag polylines ($\theta_u = \pm\pi/6$) and the subgraph G_2 is a vertical path graph ($\theta_v = \pi/2$). The lengths of the boundary edges are

$$|\boldsymbol{u}_1| = |\boldsymbol{u}_4| = |\boldsymbol{v}_1| = |\boldsymbol{v}_2|, \quad |\boldsymbol{u}_2| = |\boldsymbol{u}_3| = 0.5|\boldsymbol{v}_2|, \\ |\boldsymbol{u}_5| = |\boldsymbol{u}_6| = 0.6|\boldsymbol{v}_2| \tag{27}$$

It is easy to observe that the Cartesian product $G_1 \square G_2$ of the independent subgraphs G_1 and G_2 forms a trivial origami pattern because each boundary node necessarily satisfies the flat-foldability condition given in Eq. (8). Besides, a few non-trivial solutions can be obtained by the proposed method within 950 iteration steps. Two feasible flat-foldable patterns are shown in Figs. 13(*b*) and 13(*c*). On the other hand, some acceptable solutions can be obtained by using the existing GA method, which generally requires 765 steps. We verify that the PSO method gets more accurate results for these complex patterns than the GA method, as best function values obtained by the PSO and GA methods are, respectively, $f = 0.0062$ and $f = 0.097$.

To further evaluate the performance of the optimization model, and inspired by the $pgg_{6,2}$ non-isomorphic derivative of the Miura-ori [44,52], we examine a unit fragment with complex geometry as shown in Fig. 14(*a*). Although the directions of the vectors along the boundary are different from each other, they are verified to satisfy the flat-foldability constraint for the intersecting boundary nodes, given by

$$\theta_{u_1} + \theta_{u_6} + \pi - \theta_{v_1} - \theta_{v_2} = -60.7 \text{ deg} + 68.2 \text{ deg} \\ + 180 \text{ deg} - 81.5 \text{ deg} - 106 \text{ deg} = 0 \tag{28}$$

In addition, the lengths of these boundary edges are

$$|\boldsymbol{u}_1| = |\boldsymbol{u}_4| = 0.8|\boldsymbol{v}_2|, \quad |\boldsymbol{u}_2| = |\boldsymbol{u}_5| = 1.31|\boldsymbol{v}_2|, \\ |\boldsymbol{u}_3| = |\boldsymbol{u}_6| = 2.85|\boldsymbol{v}_2|, \quad |\boldsymbol{v}_1| = 1.85|\boldsymbol{v}_2| \tag{29}$$

Notably, there is no trivial solution for the given fragment with complex geometry, as the internal vertices obtained from the Cartesian product of the subgraphs do not satisfy the flat-foldability condition. However, by using the predetermined unit fragment and implementing the proposed optimization process, we can obtain a non-trivial solution. The corresponding origami pattern is shown in Fig. 14(*b*). Each four-fold vertex is proved to be flat-foldable, whilst the fold lines of the fragment are not parallel to each other. Moreover, the global flat-foldability of the obtained pattern is verified by a nonlinear folding analysis, where typical configurations of the tessellation, composed of 3×4 unit fragments, are shown in Fig. 15.

In comparison with the unit fragments shown in Figs. 9 and 13, the unit fragment shown in Fig. 14 is much more complex. Consequently, the involved optimization is computationally expensive. It needs more than 1570 iteration steps to approach the optimum pattern shown in Fig. 14(*b*) by using the PSO-based design method, while the feasible patterns shown in Fig. 13 can be

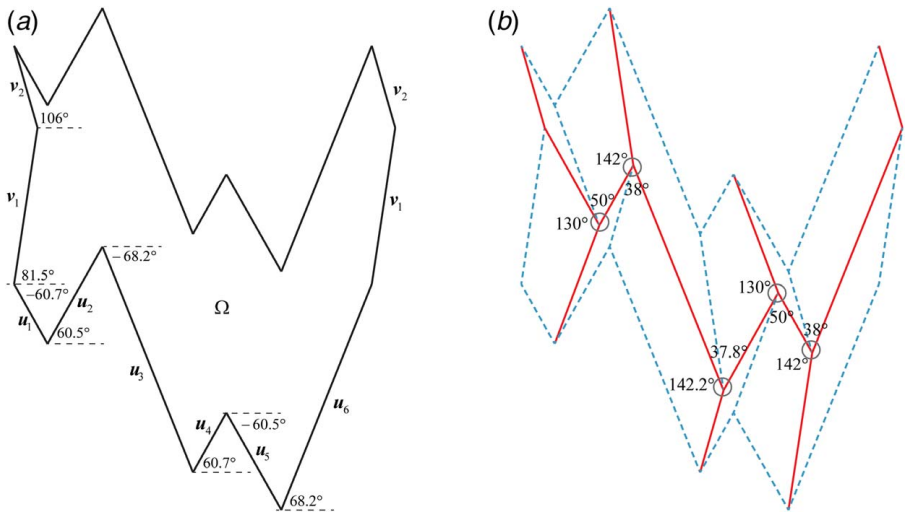

Fig. 14 A unit fragment with a complex geometry: (*a*) vectors along the boundary edges and (*b*) a flat-foldable origami pattern obtained from the optimization process

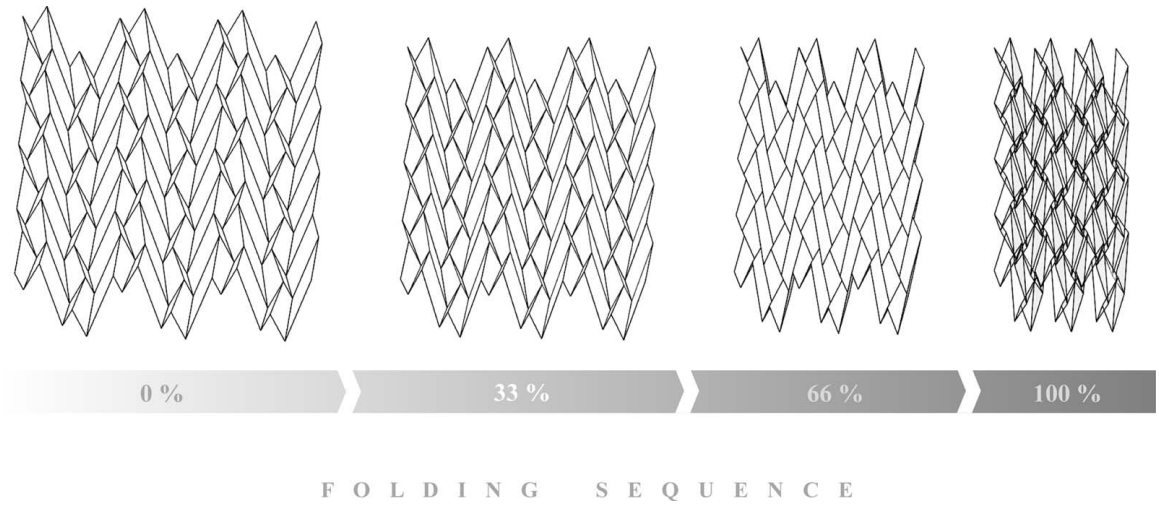

Fig. 15 Flat-folding of a $pgg_{6,2}$ derivative of the Miura-ori composed of an array of 3 × 4 unit fragments with complex boundary geometry

effectively obtained within 950 steps. It is worth mentioning that after a series of numerical implementations, the existing GA method still cannot find a feasible solution, whereas local optima are frequently obtained because of premature convergence. Thus, the proposed method is more suitable for designing complex configurations than the GA method.

Conclusions

In this study, we proposed a metaheuristic computational method for designing flat-foldable origami tessellations, capable of generating both trivial and non-trivial origami patterns with periodicity. First, the Cartesian products of two subgraphs—as the geometric-graph representations of the boundaries of the associated unit fragment—are introduced. The proposed method presents a systematic process for finding degree-4 vertices and the corresponding crease lines using a metaheuristic, inspired by the natural movement of organisms in a bird flock. To this end, a PSO method for generating origami tessellations has been established, where the flat-foldability constraint for different types of vertices is concerned.

Numerical experiments verify that the proposed method shows global and rapid convergence. For a given boundary condition, we can effectively obtain not only trivial solutions but also non-trivial flat-foldable patterns. The obtained origami patterns are proven to be feasible and flat-foldable by analytical solutions or nonlinear folding analyses. The non-trivial flat-foldable patterns, which are based on the same fragments but not easy to be obtained by certain existing methods, offer novel origami structures with different folded configurations and kinematic behavior. In comparison with the GA method using crossover and mutation operations, the proposed PSO method keeps updating the solutions through the foraging behavior of the particles. It calls for considerably fewer parameters and shows more satisfactory convergence and computational accuracy than the GA method. Our research so far enables the effective design of origami patterns with periodic symmetry. Future study will further improve the robustness of this design method for origami patterns with more complex geometries and evaluate mountain-valley fold assignments for origami patterns.

Acknowledgment

This work has been supported by the National Natural Science Foundation of China (Grant Nos. 51978150 and 51850410513), Southeast University "Zhongying Young Scholars" Project, and the Fundamental Research Funds for the Central Universities. The first author would like to acknowledge financial support from the Alexander von Humboldt-Foundation for his visiting research at Max-Planck-Institut für Eisenforschung GmbH, Germany. The authors are grateful to the editors and anonymous reviewers for their professional comments and valuable suggestions in improving the quality of the paper.

Conflict of Interest

There are no conflicts of interest.

References

[1] Gjerde, E., 2008, *Origami Tessellations: Awe-Inspiring Geometric Designs*, AK Peters/CRC Press, Boca Raton, FL.
[2] Chen, Y., Feng, J., and Sun, Q., 2018, "Lower-Order Symmetric Mechanism Modes and Bifurcation Behavior of Deployable Bar Structures With Cyclic Symmetry," Int. J. Solids Struct., **139–140**(5), pp. 1–14.
[3] Chen, Y., and Feng, J., 2012, "Folding of a Type of Deployable Origami Structures," Int. J. Struct. Stab. Dyn., **12**(6), p. 1250054.
[4] Rivas-Adrover, E., 2018, "A New Hybrid Type of Deployable Structure: Origami-Scissor Hinged," J. Int. Assoc. Shell Spatial Struct., **59**(3), pp. 183–190.
[5] Martínez-Martín, F. J., and Thrall, A. P., 2014, "Honeycomb Core Sandwich Panels for Origami-Inspired Deployable Shelters: Multi-Objective Optimization for Minimum Weight and Maximum Energy Efficiency," Eng. Struct., **69**(6), pp. 158–167.
[6] Sorguç, A. G., Hagiwara, I., and Selcuk, S., 2009, "Origamics in Architecture: A Medium of Inquiry for Design in Architecture," METU J. Fact. Archit., **26**(2), pp. 235–247.
[7] Pesenti, M., Masera, G., and Fiorito, F., 2018, "Exploration of Adaptive Origami Shading Concepts Through Integrated Dynamic Simulations," J. Archit. Eng., **24**(4), p. 04018022.
[8] Pinson, M. B., Stern, M., Ferrero, A. C., Witten, T. A., Chen, E., and Murugan, A., 2017, "Self-Folding Origami at Any Energy Scale," Nat. Commun., **8**, p. 15477.
[9] Johnson, M., Chen, Y., Hovet, S., Xu, S., Wood, B., Ren, H., Tokuda, J., and Tse, Z. T. H., 2017, "Fabricating Biomedical Origami: A State-of-the-Art Review," Int. J. Comput. Assist. Radiol. Surg., **12**(11), pp. 2023–2032.
[10] Ishikawa, N., Watanabe, G., Hirano, Y., Inaki, N., Kawachi, K., and Oda, M., 2007, "Origami Using da Vinci Surgical System," Surg. Endosc., **21**(7), pp. 1252–1253.
[11] Saccà, B., Ishitsuka, Y., Meyer, R., Sprengel, A., Schöneweiß, E. C., Nienhaus, G. U., and Niemeyer, C. M., 2015, "Reversible Reconfiguration of DNA Origami Nanochambers Monitored by Single-Molecule FRET," Angew. Chem., Int. Ed., **54**(12), pp. 3592–3597.
[12] Brittain, S. T., Schueller, O. J., Wu, H., Whitesides, S., and Whitesides, G. M., 2001, "Microorigami: Fabrication of Small, Three-Dimensional, Metallic Structures," J. Phys. Chem. B, **105**(2), pp. 347–350.
[13] Paez, L., Agarwal, G., and Paik, J., 2016, "Design and Analysis of a Soft Pneumatic Actuator With Origami Shell Reinforcement," Soft Robot., **3**(3), pp. 109–119.
[14] Pagano, A., Yan, T., Chien, B., Wissa, A., and Tawfick, S., 2017, "A Crawling Robot Driven by Multi-Stable Origami," Smart Mater. Struct., **26**(9), p. 094007.

[15] Sareh, P., Chermprayong, P., Emmanuelli, M., Nadeem, H., and Kovac, M., 2018, "Rotorigami: A Rotary Origami Protective System for Robotic Rotorcraft," Sci. Robot., **3**(22), p. eaah5228.

[16] Nagpal, R., 2001, *Programmable Self-Assembly: Constructing Global Shape Using Biologically-Inspired Local Interactions and Origami Mathematics*, Massachusetts Institute of Technology, Cambridge, MA.

[17] Balkcom, D. J., and Mason, M. T., 2008, "Robotic Origami Folding," Int. J. Robot. Res., **27**(5), pp. 613–627.

[18] Martinez, R. V., Fish, C. R., Chen, X., and Whitesides, G. M., 2012, "Elastomeric Origami: Programmable Paper-Elastomer Composites as Pneumatic Actuators," Adv. Funct. Mater., **22**(7), pp. 1376–1384.

[19] Fuchi, K., Buskohl, P. R., Bazzan, G., Durstock, M. F., Reich, G. W., Vaia, R. A., and Joo, J. J., 2015, "Origami Actuator Design and Networking Through Crease Topology Optimization," ASME J. Mech. Des., **137**(9), p. 091401.

[20] Silverberg, J. L., Jun-Hee, N., Evans, A. A., Bin, L., Hull, T. C., Santangelo, C. D., Lang, R. J., Hayward, R. C., and Itai, C., 2015, "Origami Structures With a Critical Transition to Bistability Arising From Hidden Degrees of Freedom," Nat. Mater., **14**(4), pp. 389–393.

[21] Yang, J., and Yasuda, H., 2015, "Reentrant Origami-Based Metamaterials With Negative Poisson's Ratio and Bistability," Phys. Rev. Lett., **114**(18), p. 185502.

[22] Fang, H., Chu, S. C. A., Xia, Y., and Wang, K. W., 2018, "Programmable Self-Locking Origami Mechanical Metamaterials," Adv. Mater., **30**(15), p. 1706311.

[23] Wei, Z. Y., Guo, Z. V., Dudte, L., Liang, H. Y., and Mahadevan, L., 2013, "Geometric Mechanics of Periodic Pleated Origami," Phys. Rev. Lett., **110**(21), pp. 325–329.

[24] Zhai, Z., Wang, Y., and Jiang, H., 2018, "Origami-Inspired, On-Demand Deployable and Collapsible Mechanical Metamaterials With Tunable Stiffness," Proc. Natl. Acad. Sci. USA, **115**(9), pp. 2032–2037.

[25] Zhao, Z., Kuang, X., Wu, J., Zhang, Q., Paulino, G. H., Qi, H. J., and Fang, D., 2018, "3D Printing of Complex Origami Assemblages for Reconfigurable Structures," Soft Matter, **14**(39), pp. 8051–8059.

[26] Nojima, T., 2002, "Modelling of Folding Patterns in Flat Membranes and Cylinders by Origami," JSME Int. J. C—Mech. Syst. Mach. Elem. Manuf., **45**(1), pp. 364–370.

[27] Lang, R. J., 2011, *Origami Design Secrets: Mathematical Methods for an Ancient art*, AK Peters/CRC Press, Boca Raton, FL.

[28] Lang, R. J., 2018, *Twists, Tilings, and Tessellations: Mathematical Methods for Geometric Origami*, CRC Press, Boca Raton, FL.

[29] Demaine, E. D., and O'Rourke, J., 2007, *Geometric Folding Algorithms: Linkages, Origami, Polyhedra*, Cambridge University Press, New York.

[30] Li, S., Fang, H., Sadeghi, S., Bhovad, P., and Wang, K. W., 2019, "Architected Origami Materials: How Folding Creates Sophisticated Mechanical Properties," Adv. Mater., **31**(5), p. 1805282.

[31] Chen, Y., Yan, J., and Feng, J., 2019, "Geometric and Kinematic Analyses and Novel Characteristics of Origami-Inspired Structures," Symmetry, **11**(9), p. 1101.

[32] Belcastro, S. M., and Hull, T. C., 2002, "Modelling the Folding of Paper Into Three Dimensions Using Affine Transformations," Linear Algebra Appl., **348**(PII S0024-3795(01)00608-5), pp. 273–282.

[33] Tachi, T., 2009, "Generalization of Rigid Foldable Quadrilateral Mesh Origami," J. Int. Assoc. Shell Spatial Struct., **50**(162), pp. 173–179.

[34] Zhou, X., Wang, H., and Zhong, Y., 2015, "Design of Three-Dimensional Origami Structures Based on a Vertex Approach," Proc. Royal Soc. A, **471**(2181), p. 20150407.

[35] Zirbel, S. A., Lang, R. J., Thomson, M. W., Sigel, D. A., Walkemeyer, P. E., Trease, B. P., Magleby, S. P., and Howell, L. L., 2013, "Accommodating Thickness in Origami-Based Deployable Arrays," ASME J. Mech. Des., **135**(11), p. 111005.

[36] Chen, Y., Peng, R., and You, Z., 2015, "Origami of Thick Panels," Science, **349**(6246), pp. 396–400.

[37] Qiu, C., Zhang, K., and Dai, J. S., 2016, "Repelling-Screw Based Force Analysis of Origami Mechanisms," ASME J. Mech. Robot., **8**(3), p. 031001.

[38] Qiu, C., Aminzadeh, V., and Dai, J. S., 2013, "Kinematic Analysis and Stiffness Validation of Origami Cartons," ASME J. Mech. Des., **135**(11), p. 111004.

[39] Wei, G., and Dai, J. S., 2014, "Origami-Inspired Integrated Planar-Spherical Overconstrained Mechanisms," ASME J. Mech. Des., **136**(5), p. 051003.

[40] He, Z., and Guest, S. D., 2019, "On Rigid Origami I: Piecewise-Planar Paper With Straight-Line Creases," Proc. R. Soc. A, **475**(2232), p. 20190215.

[41] Zimmermann, L., and Stanković, T., 2020, "Rigid and Flat Foldability of a Degree-Four Vertex in Origami," ASME J. Mech. Robot., **12**(1), p. 011004.

[42] Fuchi, K., and Diaz, A. R., 2013, "Origami Design by Topology Optimization," ASME J. Mech. Des., **135**(11), p. 111003.

[43] Sareh, P., and Guest, S. D., 2015, "Design of Isomorphic Symmetric Descendants of the Miura-ori," Smart Mater. Struct., **24**(8), p. 085001.

[44] Sareh, P., 2014, *Symmetric Descendants of the Miura-ori*, University of Cambridge, UK.

[45] Sareh, P., and Guest, S. D., 2015, "A Framework for the Symmetric Generalisation of the Miura-ori," Int. J. Space Struct., **30**(2), pp. 141–152.

[46] Chen, Y., Sareh, P., Yan, J., Fallah, A. S., and Feng, J., 2019, "An Integrated Geometric-Graph-Theoretic Approach to Representing Origami Structures and Their Corresponding Truss Frameworks," J. Mech. Des., **141**(9), p. 091402.

[47] Sareh, P., 2019, "The Least Symmetric Crystallographic Derivative of the Developable Double Corrugation Surface: Computational Design Using Underlying Conic and Cubic Curves," Mater. Des., **183**, p. 108128.

[48] Chen, Y., Fan, L., and Feng, J., 2017, "Kinematic of Symmetric Deployable Scissor-Hinge Structures With Integral Mechanism Mode," Comput. Struct., **191**, pp. 140–152.

[49] McAdams, D. A., and Li, W., 2014, "A Novel Method to Design and Optimize Flat-Foldable Origami Structures Through a Genetic Algorithm," J. Comput. Inf. Sci. Eng., **14**(3), p. 031008.

[50] Hull, T., 1994, "On the Mathematics of Flat Origamis," Congressus Numerantium, **100**, pp. 215–224.

[51] Kawasaki, T., 1991, "On the Relation Between Mountain-Creases and Valley-Creases of a Flat Origami," Proceedings of the First International Meeting of Origami Science and Technology, Ferrara, Italy, pp. 229–237.

[52] Sareh, P., and Guest, S. D., 2015, "Design of Non-Isomorphic Symmetric Descendants of the Miura-ori," Smart Mater. Struct., **24**(8), p. 085002.

[53] Sareh, P., and Guest, S. D., 2014, "Designing Symmetric Derivatives of the Miura-ori," Adv. Archit. Geom., pp. 233–241.

[54] Chen, Y., Yan, J., Sareh, P., and Feng, J., 2019, "Nodal Flexibility and Kinematic Indeterminacy Analyses of Symmetric Tensegrity Structures Using Orbits of Nodes," Int. J. Mech. Sci., **155**, pp. 41–49.

[55] Chen, Y., Yan, J., and Feng, J., 2019, "Stiffness Contributions of Tension Structures Evaluated From the Levels of Components and Symmetry Subspaces," Mech. Res. Commun., **100**, p. 103401.

[56] Sareh, P., and Guest, S. D., 2012, "Tessellating Variations on the Miura Fold Pattern," IASS-APCS Symposium, Seoul, South Korea, May 21–24.

[57] Chen, Y., and Feng, J., 2016, "Improved Symmetry Method for the Mobility of Regular Structures Using Graph Products," J. Struct. Eng., **142**(9), p. 04016051.

[58] Eberhart, R. C., Shi, Y., and Kennedy, J., 2001, *Swarm Intelligence*, Elsevier, New York.

[59] Kaveh, A., and Zolghadr, A., 2014, "Democratic PSO for Truss Layout and Size Optimization With Frequency Constraints," Comput. Struct., **130**, pp. 10–21.

[60] Kennedy, J., and Eberhart, R., 1995, "Particle Swarm Optimization (PSO)," Proceedings of the IEEE International Conference on Neural Networks, Perth, Australia, pp. 1942–1948.

[61] Acharyya, S. K., and Mandal, M., 2009, "Performance of EAs for Four-Bar Linkage Synthesis," Mech. Mach. Theory, **44**(9), pp. 1784–1794.

[62] Chen, Y., Yan, J., Sareh, P., and Feng, J., 2020, "Feasible Prestress Modes for Cable-Strut Structures With Multiple Self-Stress States Using Particle Swarm Optimization," J. Comput. Civil Eng., **34**(3), p. 04020003.

[63] Ghassaei, A., Demaine, E. D., and Gershenfeld, N., 2018, "Fast, Interactive Origami Simulation Using GPU Computation," 7th International Meeting on Origami in Science, Mathematics and Education, Oxford, UK, Sept. 5–7.